Optical properties and tunable luminescence of Ce^{3+}/Dy^{3+} doped lithium borate glasses for photonic applications

Bohdan Mahlovanyi[1,2], Michael Truax[3], Andriy Luchechko[2],
Yaroslav Shpotyuk[1,2], Guang Yang[4], Roman Golovchak[3], Andriy Kovalskiy[3], Jozef Cebulski[1]

[1]*Institute of Physics, University of Rzeszow, 35-959 Rzeszow, Poland*
[2]*Department of Sensory and Semiconductor Electronics, Ivan Franko National University of Lviv, 79000 Lviv, Ukraine*
[3]*Department of Physics, Engineering and Astronomy, Austin Peay State University, Clarksville, TN 37044, USA*
[4]*School of Materials Science and Engineering, Shanghai University, 200444 Shanghai, China*

Corresponding authors e-mails:
yshpotyuk@ur.edu.pl, guangyang@shu.edu.cn

Abstract

Optical absorption and photoluminescence properties of novel lithium borate glasses, (B_2O_3)-(MO)-(Li_2O)–(Bi_2O_3) where M stands for Ca, Mg or Sr, doped with Dy and Ce ions have been investigated. The fundamental optical absorption edge of these materials is observed in the region of 315-390 nm, and depends on the nature of alkaline-earth metals used as network modifiers. The photoluminescence spectra of Dy-doped glasses reveal two intensive emission bands in the visible range, which correspond to $^4F_{9/2} \rightarrow {}^6H_{15/2}$ (486 nm) and $^4F_{9/2} \rightarrow {}^6H_{13/2}$ (580 nm) transitions of Dy^{3+} ions. Ce-doped glasses show one broad band in the visible range, which corresponds to the $^2D \rightarrow {}^2F_{5/2}$ (340 nm) transition of Ce^{3+} ions. Three photoluminescence lines (980 nm, 1010 nm and 1150 nm) attributed to the Dy^{3+} ions electronic transitions are observed in the near-IR region of the spectrum for Dy-doped glasses, while only one at 1150 nm is observed for the Dy/Ce co-doped glasses. Peculiarities of excitation energy transfer between rare-earth activator ions are discussed. These glasses are shown to be a promising host matrix for rare-earth doping.

Keywords: borate glasses, luminescence, cerium, dysprosium, WLED.

1. Introduction

Borate glasses have a wide range of applications due to their simple and inexpensive production technology as well as high ability to incorporate rare earth ions, which makes them effective phosphors [1-6]. Attractive photoluminescence properties of rare earth doped borates create opportunities for their use as active media for laser technology and light sources, especially for the white light emitting device (WLED) application [5-8]. Rare earth (RE) doped glasses, in general, are cheaper in production and possess better ability for chemical modification than crystalline analogs, additionally showing better homogeneity, optical transparency in the visible and infrared regions, molding flexibility, etc [8,9].

Lithium-bismuth borate glasses (B_2O_3)-(MO)-(Li_2O)–(Bi_2O_3) with alkaline-earth oxides (M=Mg, Ca, Sr) possess high chemical stability and transparency in visible and near infra-red (NIR) optical regions [4,6]. Alkaline-earth metals can play role of the glass network formers as well as network modifiers depending on the composition [1]. Alkali metals, such as Li, Na and K, are usually used as network modifiers to improve fundamental properties of oxide glasses, reduce their melting and glass transition temperatures, viscosity, increase chemical durability, ionic conductivity, etc. [1]. Doping of borate glasses with rare-earth metals turns them into active materials, which can significantly increase their use in optoelectronics [1-7]. Large Bi atoms are highly polarizable leading to a high degree of asymmetry in the cation-oxygen polyhedral, which helps the overall glass formation [10].

Cerium and dysprosium ions in the valence state 3+ are promising luminescent centers for the development of WLEDs [11,12]. Dy^{3+} ions possess two sharp emission bands in blue and yellow regions of optical spectrum due to $^4F_{9/2}\rightarrow{}^6H_{15/2}$ and $^4F_{9/2}\rightarrow{}^6H_{13/2}$ electronic transitions, respectively. As a result, Dy^{3+} can emit white light as the combined emission from the blue and yellow bands. Ce^{3+} ions exhibit a broad luminescence band in the near ultraviolet region, which is attributed to the

$5d^1 \rightarrow 4f^1$ ($^2D \rightarrow {}^2F_{5/2}$) transition [12,13]. So, Ce^{3+} and Dy^{3+} co-doping of the borate glasses has a potential to improve their luminescent properties. In particular, Ce^{3+} ions can play a role of a dynamic sensitizer for Dy^{3+} ions. Due to the overlap of Ce^{3+} ions emission with Dy^{3+} ions absorption, cerium can effectively excite dysprosium ions [12,13].

In the present work, the photoluminescence properties of novel stable vitreous materials based on Bi-modified alkaline-earth lithium-borate (B_2O_3)-(MO)-(Li_2O)–(Bi_2O_3) glasses (M=Mg, Ca, Sr) doped with Ce and Dy, as well as co-doped with Ce/Dy have been comprehensively studied, and the materials are proposed as a new type of tunable efficient phosphors for WLEDs application [5-8]. The luminescence properties and CIE (Commission Internationale de l'éclairage, 1931) chromaticity coordinates have been analyzed, and the energy transfer processes between the rare earth ions have been discussed in terms of radiative and non-radiative transitions.

2. Experimental details

2.1. The glass synthesis and samples preparation

The Ce^{3+} or Dy^{3+} - doped and Ce^{3+}/Dy^{3+} co-doped Bi-modified lithium-borate glasses of $(B_2O_3)_{58}(MO)_{20}(Li_2O)_{20}(Bi_2O_3)_{2-x}(RE)_x$ composition, where M=Mg, Ca, Sr; RE= CeO_2, Dy_2O_3 and x=0 or 1, were prepared using melt quenching technique and powder of high purity precursors: H_3BO_3 (Honeywell, 98.5), $SrCO_3$ (Chempur, 99.9%), $CaCO_3$ (Honeywell, 98.5), Li_2CO_3 (AlfaAesar, 99.998%), MgO (AlfaAesar, 99.95 %), Bi_2O_3 (AlfaAesar, 99,99%), CeO_2 (AlfaAesar, 99,99%), Dy_2O_3 (AlfaAesar, 99.99%). The compositions of the studied glasses are shown in Table 1. The synthesis was performed under an air atmosphere in Al_2O_3 ceramic crucibles, using a programmable furnace (4 h heating up to 600 ºC with dwell for 30 min, followed by 2h heating to 800 ºC with dwell for 30 min to avoid rapid expansion of the batch, and finally heating during 2 h to 1100 ºC and dwell

for 1 h). The melt was swiftly quenched into carbon mold. In the last stage, the samples were annealed in the air atmosphere for 4 h at 400 °C to relieve the internal stresses appeared as a result of rapid quenching.

2.2. Characterization methods

The density has been measured in ethanol using Archimedes principle:

$$\rho = \rho_x \frac{W_a}{W_a - W_x} \quad (1)$$

where ρ_x is the density of ethanol, W_a is the weight of the sample in air and W_x is the weight in ethanol. The molar volume (V_m) has been calculated as $V_m = M/\rho$ where M is a molecular weight of the sample.

Optical transmission spectra were recorded with 2 nm resolution in 200 – 3200 nm spectral range, using Agilent Technologies Cary-5000 UV-Vis-NIR spectrometer and bulk samples polished to a high optical quality.

Raman spectra were obtained with a Renishaw inVia Raman Microscope in the frequency range of 50 – 2000 cm^{-1}. Argon laser Stellar-REN with a wavelength of 488 nm and power of 50 mW (10% of the power was set during measurements, 10 s exposure time, 2 accumulations, 50x objective) was used for excitation. Spectra were obtained in a reflection mode at room temperature.

Photoluminescence measurements were carried out on a CM2203 spectrofluorometer in the 220-820 nm spectral range. All luminescence spectra were obtained with a spectral resolution of 1 nm. Excitation of luminescence was performed with a 150 W xenon lamp. A Hamamatsu R928 photomultiplier was used as a luminescence detector. The 3D luminescence maps in the near-IR region of the spectrum were obtained at room (T_R = 298 K) temperature, using Horiba Fluorolog-3 spectrofluorimeter equipped with a xenon short arc lamp as a light excitation source. The emission spectra were collected in the 850-1600 nm range using liquid nitrogen-cooled Horiba Jobin Yvon InGaAs DSS-IGA020L detector.

3. Results and discussion

The impact of CeO_2 and Dy_2O_3 doping on the visual color of the prepared glasses is shown in Figure 1. As it can be seen, all glasses are homogeneous and bubbles-free. Their physical properties, such as thickness *d*, molecular weight *M,* density ρ, and molar volume V_m, are presented in Table 2.

The density of undoped glasses increases when alkaline-earth metal Mg is replaced with Ca and then Sr. The lowest density is observed for Ce doped Mg-based glass (Mg3:Ce1) and the highest one is recorded for Sr-based Dy doped glass (Sr2:Dy1 sample). The increase and decrease of the V_m value could be explained by the formation of Bi-O and RE-O bonds and non-bridging oxygens, which affect the amount of free volume in the structure of borate glasses [10,14,15].

3.1. Structural properties – Raman spectroscopy

Figure 2 shows Raman spectra of undoped $(B_2O_3)_{58}(MO)_{20}(Li_2O)_{20}(Bi_2O_3)_2$ (M=Mg, Ca, Sr) glasses. The spectra show strong bands at 1400 cm^{-1}, 1020 cm^{-1}, 900 cm^{-1}, 768 cm^{-1}, 511 cm^{-1}, and two weaker bands at ~370 cm^{-1} and 663 cm^{-1}. The broad band at 1400 cm^{-1} is related to stretching vibrations of non-bridging oxygen $B\text{-}O^-$ bonds attached to larger borate groups [16]. Peaks with maxima of around 1020 cm^{-1} and 900 cm^{-1} have contribution from B-O bond stretching of BO_4^- tetraborate and pentaborate units [16-18]. The peak near 1020 cm^{-1} is changing with alkaline-earth substitution and shifts from 1006 cm^{-1} for glass with Mg to 1026 cm^{-1} for glass with Sr. So, it must also contain a vibrational mode from units containing/neighboring to these alkaline-earth network modifiers. The peak at 768 cm^{-1} is assigned to breathing vibrations of six-member borate rings with one or two BO_3 triangles replaced with BO_4 tetrahedra, whereas a shoulder at 663 cm^{-1} can be attributed to ring and/or chain metaborate groups and $BO_2O_2^{3-}$ units [16,19]. Another low-frequency peak at 511 cm^{-1} with a shoulder centered at ~372 cm^{-1} may be caused by "isolated" diborate units as well as Bi-O-Bi bond vibrations in BiO_6 octahedral units [20].

3.2. *Optical transmission spectra of the studied borate glasses*

The optical transmission spectra of undoped glasses are presented in Figure 3a, showing the fundamental optical absorption edge at ~320 nm.

Figures 3b-f show the transmission spectra of Ce- and Dy-doped Bi-modified lithium-borate glasses. Dy-doped glasses (Fig. 3 b-c) have strong absorption bands due to Dy^{3+} ions, which correspond to the electronic transitions from $^6H_{15/2}$ ground state to higher electronic states. These bands are located at 348, 364, 386, 388, 426, 450, 474, 796, 894, 1088, 1262 and 1676 nm. In contrast to the transmission spectra of Dy–doped samples, Ce-doped glasses (Fig. 3 d, e) do not show any absorption bands in the entire transmission range. Furthermore, the beginning of transmission is noticeably shifted from 320 nm, as observed for the undoped and Dy-doped glasses, towards longer wavelengths at ~375 nm for Ce-doped and Dy /Ce co-doped samples (Fig. 3 f). This is due to the optical absorption of Ce that emerges as a wide band extending from the UV to the visible region [21].

The obtained transmission curves were used to calculate the absorption coefficient (Fig. 4a-c) and estimate optical band gap ΔE_{opt} using Tauc plots for indirect transitions in the PARAV program [22]. The calculated values of the band gap are given in Table 3. As expected, the value of the band gap varies and depends on the composition of the glass matrix and the nature of the dopants. The trend of optical gap increase is observed when Mg network modifier is replaced with Ca and then with Sr (Table 3). Replacing of Bi with Dy dopant leads to an increase of ΔE_{opt}, while the introduction of Ce instead decreases this value significantly (Table 3).

3.3. Photoluminescent properties in the visible range

The photoluminescence spectra of Dy- and Ce-doped lithium borate glasses are shown in Fig. 5 (a,b). The emission spectra of Dy-doped glasses (Fig. 5 a) under 350 nm excitation have two strong visible emission bands located at 486 nm (blue) and 579 nm (yellow), which correspond to a

magnetic dipole ($^4F_{9/2}\rightarrow{}^6H_{15/2}$) and electric dipole ($^4F_{9/2}\rightarrow{}^6H_{13/2}$) transitions, respectively [12,13]. In addition to the mentioned two intense peaks, the spectrum also shows two low-intensity emission bands at 458 nm and 667 nm, corresponding to $^4I_{15/2}\rightarrow{}^6H_{15/2}$ and $^4F_{9/2}\rightarrow{}^6H_{11/2}$ transitions [12,13].

It is well known that a form of the emission spectrum reflects the local symmetry of rare earth ions in the lattice. The magnetic dipole transition usually dominates for the ion in a site with higher symmetry, while electric dipole transitions are normally attributed to the ions in sites with lower symmetry [23-25]. The important parameter that can be used to identify the symmetry site of Dy^{3+} ions in glasses is the intensity ratio (I_{579}/I_{486}) between electric dipole (intensity I_{579} of 579 nm yellow line) and magnetic dipole (intensity I_{486} of 486 nm blue line) transitions. The calculated I_{579}/I_{486} ratio is equal to 0.66 for Mg2:Dy1, 0.69 for Ca2:Dy1, and 0.69 for Sr2:Dy1 glasses. For comparison, this ratio is in the range of 1.40÷1.43 for the Dy-doped B_2O_3-SiO_2-Gd_2O_3-CaO glasses, depending on the concentration of the dopant [25]. The obtained ratios indicate that highly symmetric environments around Dy^{3+} emission ions are dominated in all three types of glasses.

Photoluminescence spectra of Ce-doped borate glasses (Fig. 5 b) under 270 nm excitation show one broad band at 360 nm (356 nm for Mg3:Ce1) related to $^2D\rightarrow{}^2F_{5/2}$ transition of Ce^{3+} ions [9,11]. Nevertheless, all three types of glass prove to be effective hosts for rare earth elements. Broad emission bands of Ce^{3+} ions originated from 4*f*-5*d* electric-dipole transitions extend from UV into the visible region, which makes cerium a possible dynamic sensitizer for certain rare earth ions [11,12]. Thus, Ce^{3+} ions can excite Dy^{3+} ions because of a substantial overlap between the emission of Ce^{3+} ion and 4*f* - 4*f* absorption of Dy^{3+} ion [11-13,26], which is demonstrated in Fig. 6.

The luminescence yield correlates with light emission efficiency and can be estimated by comparing the luminescence intensity at specific wavelengths in each sample. As can be seen from the figures, the intensity of Dy^{3+} ions is weakly correlated with the content of Mg/Ca/Sr in the glasses

(Fig. 5a). At the same time, the intensity of Ce^{3+} luminescence in Ca3:Ce1 glasses is the highest (Fig. 5b). It decreases by approximately 16% for Sr3:Ce1 and 27% for Mg3:Ce1.

The energy level diagram, which reflects the transfer of excitation energy from Ce^{3+} to Dy^{3+} ions as well as the absorption and the emission transitions of these ions, is shown in Fig. 7. It should be noted that the electronic transitions presented in this diagram correlate with the results presented in the Figures 3-6. In particular, part of the Ce^{3+} ions emission energy can be absorbed by the Dy^{3+} ions (Fig. 6). As a result, the electrons from the ground state $^6H_{15/2}$ are excited to the $^4F_{7/2} + {}^4I_{13/2}$ or higher levels. Then the electrons can non-radiatively relax to the $^4F_{9/2}$ level, further giving the blue and yellow emissions of Dy^{3+} ions, enhancing the emission intensity of Dysprosium accordingly.

Photoluminescence spectra of alkaline-earth Bi-modified lithium-borate glasses co-doped with 0.5 mol% of CeO_2 and Dy_2O_3 under 270 nm excitation are presented in Fig. 8. Spectra consists of broad emission bands of Ce^{3+} ions peaking at 340 nm for Mg4:(Ce,Dy)0.5 glass, 354 nm for Ca4:(Ce,Dy)0.5 and 359 nm for Sr4:(Ce,Dy)0.5 glasses, which can be attributed to $^2D \rightarrow {}^2F_{5/2}$ transition. The following two narrower peaks at 486 and 579 nm are attributed to $^4F_{9/2} \rightarrow {}^6H_{15/2}$ and $^4F_{9/2} \rightarrow {}^6H_{13/2}$ transitions of Dy^{3+}, respectively. These peaks of Dy^{3+} ions may be a consequence of energy transfer from cerium ions excited by UV radiation of 270 nm to the excited energy levels of dysprosium ions. Under this UV excitation, a part of the Ce^{3+} ions in the glass absorbs the energy and emits light at around 350 nm during their transition to the ground $^2F_{5/2}$ state. At the same time, the rest of the Ce^{3+} ions transfer their energy to Dy^{3+} ions. The excited Dy^{3+} ions undergo non-radiative transitions or multiphonon relaxations, eventually populating the $^4F_{9/2}$ and $^4I_{15/2}$ energy levels. These energy levels are responsible for the visible emission of Dy^{3+} ions, leading to the blue and yellow emissions observed in the photoluminescence spectra (Fig. 5a).

Overall, the $Ce^{3+} \rightarrow Dy^{3+}$ energy transfer mechanism observed in the co-doped lithium borate glasses enhances the luminescent properties of the material, leading to efficient visible emissions. This

makes studied glasses a promising candidate for applications in different phosphors and other optoelectronic devices. Further studies and optimization of the glass composition may lead to the development of phosphors with more efficient energy transfer and improved luminescence properties, making these glasses even more suitable for various technological applications.

3.4. Chromaticity diagram analysis

CIE 1931 chromaticity diagram, as shown in Figure 9, provides essential information about the color properties of the studied borate glasses. The color coordinates (x, y), correlated color temperature (CCT), and color purity are presented in Table 4.

The Dy-doped glasses (Mg2:Dy1, Ca2:Dy1, and Sr2:Dy1) exhibit CIE coordinates close to the white light point (0.33, 0.33), indicating that they emit balanced white light. This characteristic makes them suitable candidates for applications in WLEDs and other light-emitting devices that require natural-looking illumination. In contrast, the glasses co-doped with Ce and Dy (Mg4:(Ce,Dy)0.5 and Ca4:(Ce,Dy)0.5) demonstrate total emission in the slightly blue or cold white region of the chromaticity diagram. Therefore, adding Ce^{3+} ions shifts the emission toward the blue part of the spectrum. The luminescence of the Ce^{3+}-doped glasses (Mg3:Ce1, Ca3:Ce1, and Sr3:Ce1) spans a broader range on the chromaticity diagram, indicating a wider variety of colors.

Overall, the color chromaticity diagram based on the CIE coordinates provides valuable insights into the emission properties of the studied Bi-modified lithium-borate glasses. It offers guidance for selecting the appropriate glass compositions for different lighting and optoelectronic applications that demand specific color characteristics.

The estimation of CP was carried out based on the formula presented in [27] Among the Ce-doped glasses exhibiting blue tonality the Ca3:Ce1 sample demonstrates the highest blue color purity

(74%) with a dominant wavelength of 465 nm. The tonality of the Ce/Dy - co-doped glasses can be considered bluish-white due to its low color purity ~ 20%.

3.5. Photoluminescent properties in the near-IR range

The 3D maps of photoluminescent spectra for Dy-doped and Dy/Ce co-doped lithium borate glasses are shown in Fig. 10. Undoped glasses and Ce-doped glasses did not show any significant luminescence in the entire 750-1600 nm range of near-IR emission spectrum. Dy-doped glasses show 3 emission lines: weaker at ~980 nm and ~1010 nm, and stronger at ~1150 nm (Figs. 10a,c,e). The first two emission lines correspond to $^4F_{9/2} \rightarrow {}^6F_{7/2}$ and $^4I_{15/2} \rightarrow {}^6F_{5/2}$ radiative transitions, while the third one is caused by $^4F_{9/2} \rightarrow {}^6F_{5/2}$ and/or combined $^6H_{9/2} + {}^6F_{11/2} \rightarrow {}^6H_{15/2}$ radiative transitions [28, 29] (Fig. 7). They are observed under the excitation wavelengths 286 nm, 322 nm, 348 nm, 364 nm, 388 nm and 450 nm, which correspond to $^6H_{15/2} \rightarrow {}^6P_{3/2}$, $^6H_{15/2} \rightarrow {}^6P_{7/2}$, $^6H_{15/2} \rightarrow {}^6P_{5/2}$, $^6H_{15/2} \rightarrow {}^4F_{7/2}$ and $^6H_{15/2} \rightarrow {}^4I_{15/2}$ upward transitions in Fig. 7. After these high-energy excitations, the excited electrons can undergo multiple non-radiative transitions or multiphonon relaxations populating the $^4F_{9/2}$ and $^4I_{15/2}$ energy levels, which makes possible the observed luminescence in the near-IR region. The luminescence intensity of the observed three emission lines increases when Ca is replaced with Mg and then Sr in the composition. In the Dy/Ce-co-doped glasses, a noticeable emission is observed only at 1150 nm under the same excitation wavelengths: 286 nm, 322 nm, 348 nm, 364 nm, 388 nm and 450 nm, which correspond to $^6H_{15/2} \rightarrow {}^6P_{3/2}$, $^6H_{15/2} \rightarrow {}^6P_{7/2}$, $^6H_{15/2} \rightarrow {}^6P_{5/2}$, $^6H_{15/2} \rightarrow {}^4F_{7/2}$ and $^6H_{15/2} \rightarrow {}^4I_{15/2}$ upward transitions in Fig. 7. However, contrary to Dy-doped samples, the strength of 1150 nm emission decreases when Ca is replaced with Mg and then Sr (Figs. 10b,d,f), showing opposite behavior.

4. Conclusions

Optical properties of Ce^{3+} or Dy^{3+} doped and Ce^{3+}/Dy^{3+} co-doped alkaline-earth Bi-modified lithium-borate glasses show their great potential as a novel host medium for rare earth elements. Intense broad emissions of Ce^{3+} ions in the UV part of the spectrum near 350 nm as well as the intense emission lines of Dy^{3+} ions in the visible spectral region at about 486 and 579 nm are detected with UV-Vis photoluminescence spectroscopy. The intensity ratio of the electric dipole to magnetic dipole transitions suggests that the coordination polyhedron around Dy^{3+} ions is highly symmetric in all investigated glasses. In the near-IR region of the spectrum, the photoluminescence associated with $^4F_{9/2} \rightarrow {}^6F_{7/2}$ (980 nm), $^4I_{15/2} \rightarrow {}^6F_{5/2}$ (1010 nm), and $^4F_{9/2} \rightarrow {}^6F_{5/2}$, $^6H_{9/2} + {}^6F_{11/2} \rightarrow {}^6H_{15/2}$ (both at 1150 nm) radiative transitions are observed for Dy-doped and Dy/Ce co-doped glasses. Their intensity shows significant dependence on the nature of alkaline network modifiers. The ability to control the CIE coordinates by adjusting the composition of lithium-borate glasses and/or co-doping with Ce and Dy opens up possibilities for tailoring the emission properties for different light emitting device applications. Experimental data reveal that the emission of Dy^{3+} ions in alkaline-earth borate host glasses is located in the white region (from CIE coordinates), which makes them a potential phosphor material for WLEDs. In the studied glasses, Ce^{3+} ions act as sensitizers for Dy^{3+} ions, absorbing the excitation energy and transferring part of it to the Dy^{3+} ions that emit visible light. The energy transfer from Ce to Dy can enhance and tune the visible emission properties of the host material.

CRediT authorship contribution statement

Bohdan Mahlovanyi: Conceptualization, Investigation, Writing – review & editing. **Michael Truax**: Investigation, Visualization, Writing – review & editing. **Yaroslav Shpotyuk:** Conceptualization, Investigation, Supervision, Writing – review & editing. **Andriy Luchechko**: Investigation, Visualization, Writing – review & editing. **Guang Yang:** Investigation, Visualization.

Roman Golovchak: Investigation, Visualization, Writing – review & editing. **Andriy Kovalskiy:** Conceptualization, Investigation, Writing – review & editing. **Jozef Cebulski**: Investigation, Visualization, Funding acquisition.

Declaration of competing interest

The authors declare that they have no known competing financial interests or personal relationships that could have appeared to influence the work reported in this paper.

Data availability

Data will be made available on request.

Acknowledgments

The authors acknowledge support of the National Science Foundation (NSF project OISE-2106457).

References

1. B. Karmakar, Functional glasses and glass-ceramics. Processing, properties and applications. Elsevier Inc. 2017. doi:10.1016/C2015-0-04249-6
2. Y. Kitagawa, E.G. Yukihara, S. Tanabe, Development of Ce^{3+} and Li^{+} co-doped magnesium borate glass ceramics for optically stimulated luminescence, J. Lumin. 232 (2021) 117847. doi:10.1016/j.jlumin.2020.117847

3. M.M. EL-Hady, H.Y. Morshidy, M.A. Hassan, Judd-Ofelt analysis, optical and structural features of borate glass doped with erbium oxide, J. Lumin. 263 (2023) 119972. doi:10.1016/j.jlumin.2023.119972
4. F. Steudel, A.C. Rimbach, S. Loos, B. Ahrens, S. Schweizer, Effect of induced crystallization in rare-earth doped lithium borate glass, Rad. Meas. 90 (2016) 274-278. doi:10.1016/j.radmeas.2015.12.046
5. X.B. Li, W.B. Dai, K. Nie, S.P. Li, M. Xu, Investigation on optical properties of borate $Sr_3Y_2B_4O_{12}$: Ce/Tb/Sm and its application in wLEDs, J. Lumin. 263 (2023) 120038. doi:10.1016/j.jlumin.2023.120038
6. I. Ullah, S.K. Shah, G. Rooh, N. Srisittipokakun, A. Khan, J. Kaewkhao, H.J. Kim, S. Kothan, Spectroscopic study and energy transfer behavior of Gd^{3+} to Dy^{3+} for Li_2O–MgO-Gd_2O_3–B_2O_3–Dy_2O_3 glasses for white emission material, J. Lumin. 226 (2020) 117380. doi:10.1016/j.jlumin.2020.117380
7. A. Górny, M. Kuwik, W.A. Pisarski, J. Pisarska, Lead borate glasses and glass-ceramics singly doped with Dy^{3+} for white LEDs, Mater. 13 (2020) 5022. doi:10.3390/ma13215022
8. J.M. An, D.S. Li, X.Y. He, E.Y.B. Pun, H. Lin, Revealing the multicolor mechanism in borotellurite glass phosphor: From individual emission of dual-modes to WLED applications, J. Lumin. 234 (2021) 117972. doi:10.1016/j.jlumin.2021.117972
9. V. Rajeswara Rao, L. Lakshmi Devi, C.K. Jayasankar, Wisanu Pecharapa, J. Kaewkhao, Sh.R. Depuru, Luminescence and energy transfer studies of Ce^{3+}/Dy^{3+} doped fluorophosphate glasses, J. Lumin. 208 (2019)89-98. doi: 10.1016/j.jlumin.2018.11.053
10. A.K. Varshneya, Fundamentals of inorganic glasses. Sheffield: Society of Glass Technology, 2006.

11. L. Vijayalakshmi, K. Naveen Kumar, K. Srinivasa Rao, Pyung Hwang, Tunable color emission via energy transfer in co-doped Ce^{3+}/Dy^{3+}: Li_2O-LiF-B_2O_3-ZnO glasses for photonic applications, Opt. Mater. 72 (2017) 781-787. doi:10.1016/j.optmat.2017.07.034
12. P. Zhang, Y. Pu, X. Zhu, H. Zheng, J. Zhao, Y. Wu, Y. Luo, Y. L. Zhang, Luminescence properties of Dy^{3+} doped and Dy^{3+}/Ce^{3+} co-doped CaO–Al_2O_3–SiO_2–B_2O_3 glass for LED applications, Ceram. Int. 41 (2015) S729-S733. doi:10.1016/j.ceramint.2015.03.250
13. S. Stojadinović, A. Ćirić, Dy^{3+} and Dy^{3+}/Ce^{3+} doped Al_2O_3 coatings obtained by plasma electrolytic oxidation: Photoluminescence and energy transfer from Ce^{3+} to Dy^{3+}, J. Lumin. 226 (2020) 117403. doi:10.1016/j.jlumin.2020.117403
14. S. Dubuis, S.H. Messaddeq, Y. Ledemi, A. Côté, Y. Messaddeq, Effect of Bi_2O_3 on the physical, structural and NIR emission properties of BGG glasses prepared using different melting atmospheres, Opt. Mater. Express 11 (2021) 2560-2575. doi:10.1364/OME.430811
15. Y. Saddeek, M. Gaafar, N. Abd El-Aal, L. Abd El-Latif, Structural analysis of some alkali diborate glasses, Acta Phys. Polon. A 116 (2009) 211-2169. doi:10.12693/APhysPolA.116.211
16. E. I. Kamitsos, M. A. Karakassides, G. D. Chryssikos, Vibrational spectra of magnesium-sodium-borate glasses. Raman and mid-infrared investigation of the network structure, J. Phys. Chem. 91 (1987) 1073-1079. doi:10.1021/j100289a014
17. W.L. Konijnendijk, J.M. Stevels, The structure of borate glasses studied by Raman scattering, J. Non-Cryst. Solids 18 (1975) 307-331. doi:10.1016/0022-3093(75)90137-4
18. G. Padmaja, P. Kistaiah, Infrared and Raman spectroscopic studies on alkali borate glasses: evidence of mixed alkali effect, J. Phys. Chem. A 113 (2009) 2397-2404. doi:10.1021/jp809318e
19. P. Dwivedi, B.N. Khanna, Cation dependence of Raman scattering in alkali borate glasses, J. Phys. Chem. Solids 56 (1995) 39-49. doi:10.1016/0022-3697(94)00130-8

20. M. Subhadra, P. Kistaiah, Infrared and Raman spectroscopic studies of alkali bismuth borate glasses: Evidence of mixed alkali effect, Vibr. Spectr. 62 (2012) 23-27. doi:10.1016/j.vibspec.2012.07.001

21. I.I. Kindrat, B.V. Padlyak, S. Mahlik, B. Kukliński, Y.O. Kulyk, Spectroscopic properties of the Ce-doped borate glasses, Opt. Mater. 59 (2016) 20-27. doi:10.1016/j.optmat.2016.03.053

22. A. Ganjoo, R. Golovchak, Computer program PARAV for calculating optical constants of thin films and bulk materials: Case study of amorphous semiconductors, J. Optoelectronics Adv. Materials 10 (2008) 1328-1332.

23. X. M. Zang, D. S. Li, E. Y. B. Pun, and H. Lin, Dy^{3+} doped borate glasses for laser illumination, Opt. Mater. Express 7 (2017) 2040-2054. doi:10.1364/OME.7.002040

24. A. Luchechko, Y. Shpotyuk, O. Kravets, O. Zaremba, K. Szmuc, J. Cebulski, A. Ingram, R. Golovchak, O. Shpotyuk, Microstructure and luminescent properties of Eu^{3+}-activated $MgGa_2O_4:Mn^{2+}$ ceramic phosphors, J. Adv. Ceram. 9 (2020) 432-443. doi:10.1007/s40145-020-0386-5

25. J. Kaewkhao, N. Wantana, S. Kaewjaeng, S. Kothan, H.J. Kim, Luminescence characteristics of Dy^{3+} doped Gd_2O_3-CaO-SiO_2-B_2O_3 scintillating glasses, J. Rare Earths 34 (2016) 583-589. doi:10.1016/S1002-0721(16)60065-0

26. W. He, X. Wang, J. Zheng, X. Yan, Optical property of Dy^{3+}-and Ce^{3+}-doped Si–B–Na–Sr glasses, J. Am. Ceram. Soc. 97 (2014) 1750-1755. doi:10.1111/jace.12973

27. A.U. Trápala-Ramírez, J.N.L. Gálvez-Sandoval, A. Lira, I. Camarillo, E. Alvarez-Ramos, A.N. Meza-Rocha, U. Caldiño, Calcium-zinc phosphate glasses activated with Tb^{3+}/Eu^{3+} for laser and white LED applications, J. Lumin. 215 (2019) 116621. doi:10.1016/j.jlumin.2019.116621

28. Y. Yang, L. Liu, S. Cai, F. Jiao, C. Mi, X. Su, J. Zhang, F. Yu, X. Li, Z. Li, Up-conversion luminescence and near-infrared quantum cutting in Dy^{3+}, Yb^{3+} co-doped $BaGd_2ZnO_5$ nanocrystal, J. Lumin, 146 (2014) 284-287. doi:10.1016/j.jlumin.2013.09.069

29. J. Feng, L. Zhou, S-Y. Song, Z-F. Li, W-Q. Fan, L-N. Sun, Y-N. Yu, H-J. Zhang, A study on the near-infrared luminescent properties of xerogel materials doped with dysprosium complexes, Dalton Trans. 33 (2009) 6593-6598. doi:10.1039/B906419B

Table 1. Investigated glass compositions with labels.

№	Label	Composition
1	Mg1-Bi2	$(B_2O_3)_{58}$-$(MgO)_{20}$-$(Li_2O)_{20}$-$(Bi_2O_3)_2$
2	Mg2:Dy1	$(B_2O_3)_{58}$-$(MgO)_{20}$-$(Li_2O)_{20}$-$(Bi_2O_3)_1$:$(Dy_2O_3)_1$
3	Mg3:Ce1	$(B_2O_3)_{58}$-$(MgO)_{20}$-$(Li_2O)_{20}$-$(Bi_2O_3)_1$:$(CeO_2)_1$
4	Mg4:(Ce,Dy)0,5	$(B_2O_3)_{58}$-$(MgO)_{20}$-$(Li_2O)_{20}$-$(Bi_2O_3)_1$: $(CeO_2)_{0.5}$/$(Dy_2O_3)_{0,5}$
5	Ca1-Bi2	$(B_2O_3)_{58}$-$(CaO)_{20}$-$(Li_2O)_{20}$-$(Bi_2O_3)_2$
6	Ca2:Dy1	$(B_2O_3)_{58}$-$(CaO)_{20}$-$(Li_2O)_{20}$-$(Bi_2O_3)_1$:$(Dy_2O_3)_1$
7	Ca3:Ce1	$(B_2O_3)_{58}$-$(CaO)_{20}$-$(Li_2O)_{20}$-$(Bi_2O_3)_1$:$(CeO_2)_1$
8	Ca4:(Ce,Dy)0,5	$(B_2O_3)_{58}$-$(CaO)_{20}$-$(Li_2O)_{20}$-$(Bi_2O_3)_1$: $(CeO_2)_{0.5}$/$(Dy_2O_3)_{0,5}$
9	Sr1-Bi2	$(B_2O_3)_{58}$-$(SrO)_{20}$-$(Li_2O)_{20}$-$(Bi_2O_3)_2$
10	Sr2:Dy1	$(B_2O_3)_{58}$-$(SrO)_{20}$-$(Li_2O)_{20}$-$(Bi_2O_3)_1$:$(Dy_2O_3)_1$
11	Sr3:Ce1	$(B_2O_3)_{58}$-$(SrO)_{20}$-$(Li_2O)_{20}$-$(Bi_2O_3)_1$:$(CeO_2)_1$
12	Sr4:(Ce,Dy)0.5	$(B_2O_3)_{58}$-$(SrO)_{20}$-$(Li_2O)_{20}$-$(Bi_2O_3)_1$:$(CeO_2)_{0.5}$/$(Dy_2O_3)_{0,5}$

Table 2. Physical properties of $(B_2O_3)_{58}(MO)_{20}(Li_2O)_{20}(Bi_2O_3)_{2-x}(RE)_x$ glass samples.

Sample	d, mm	ρ, g/cm^3	M, g/mol	V_m, cm^3/mol
Mg1-Bi2	2.6	2.585	63.7336	24.66
Mg2:Dy1	2.1	2.565	62.804	24.485
Mg3:Ce1	1.8	2.504	60.79521	24.28
Mg4:(Ce,Dy)0,5	2.5	2.534	61.79961	24.39
Ca1-Bi2	2	2.597	66.8882	25.76
Ca2:Dy1	2.5	2.576	65.9586	25.61
Ca3:Ce1	1.8	2.519	63.94981	25.387
Ca4:(Ce,Dy)0.5	2	2.587	64.95421	25.108
Sr1-Bi2	2	2.695	76.3966	28.346
Sr2:Dy1	2	2.731	75.467	27.633
Sr3:Ce1	2	2.642	73.45821	27.804
Sr4:(Ce,Dy)0.5	1.8	2.728	74.463	27.295

Table 3. Estimated values of the optical band gap for alkali-earth lithium borate glasses.

Sample	ΔE_{opt}, eV	Sample	ΔE_{opt}, eV	Sample	ΔE_{opt}, eV
Mg1-Bi2	3.66	Ca1-Bi2	3.69	Sr1-Bi2	3.72
Mg2:Dy1	3.77	Ca2:Dy1	3.71	Sr2:Dy1	3.79
Mg3:Ce1	3.03	Ca3:Ce1	3.06	Sr3:Ce1	3.08
Mg4:(Ce,Dy)0.5	2.99	Ca4:(Ce,Dy)0.5	3.02	Sr4:(Ce,Dy)0.5	3.03

Table 4. CIE coordinates (x, y) and correlated color temperature (CCT) of the luminescence.

Sample	x	y	CCT, K
Mg2:Dy1	0.3044	0.34197	6844
Ca2:Dy1	0.31487	0.35271	6260
Sr2:Dy1	0.31175	0.34787	6431
Mg3:Ce1	0.20692	0.15362	7591
Ca3:Ce1	0.18108	0.11276	2860
Sr3:Ce1	0.20872	0.1686	-
Mg4:(Ce,Dy)0.5	0.26815	0.28262	11733
Ca4:(Ce,Dy)0.5	0.27725	0.27919	10865

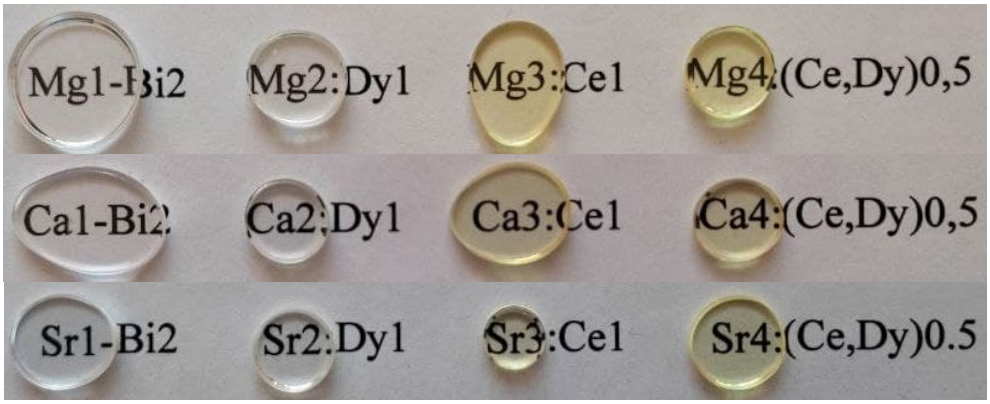

Fig. 1. Photo of the obtained series of borate glasses.

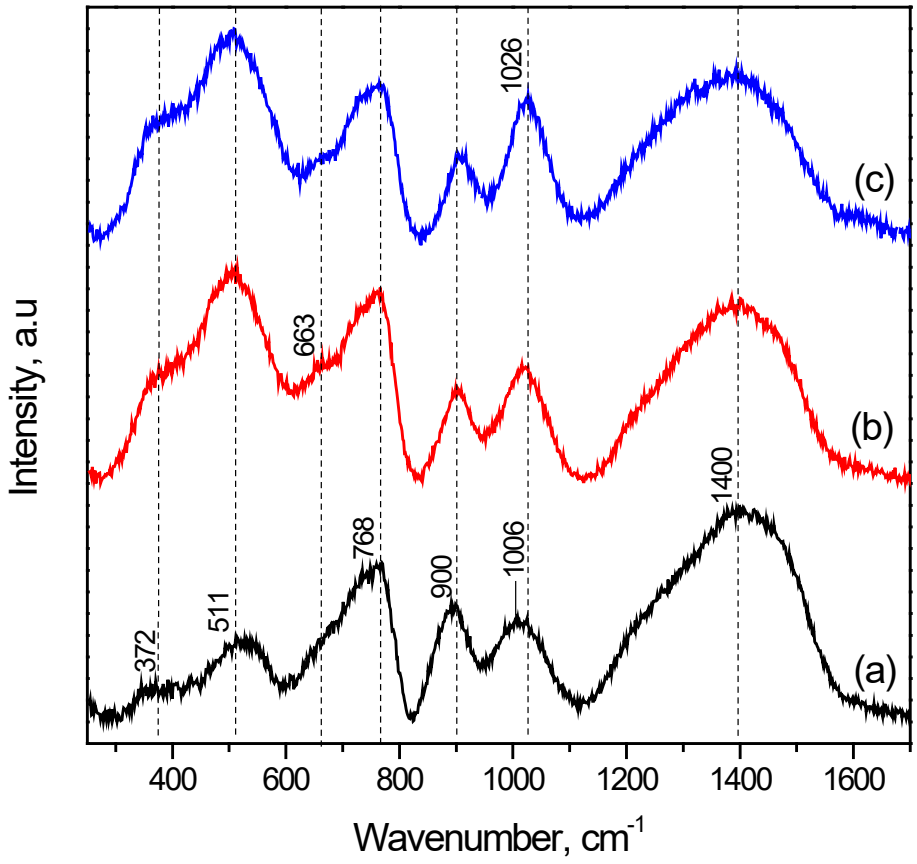

Fig. 2. Raman spectra of undoped glass samples: (a) Mg1-Bi2, (b) Ca1-Bi2, (c) Sr1-Bi2.

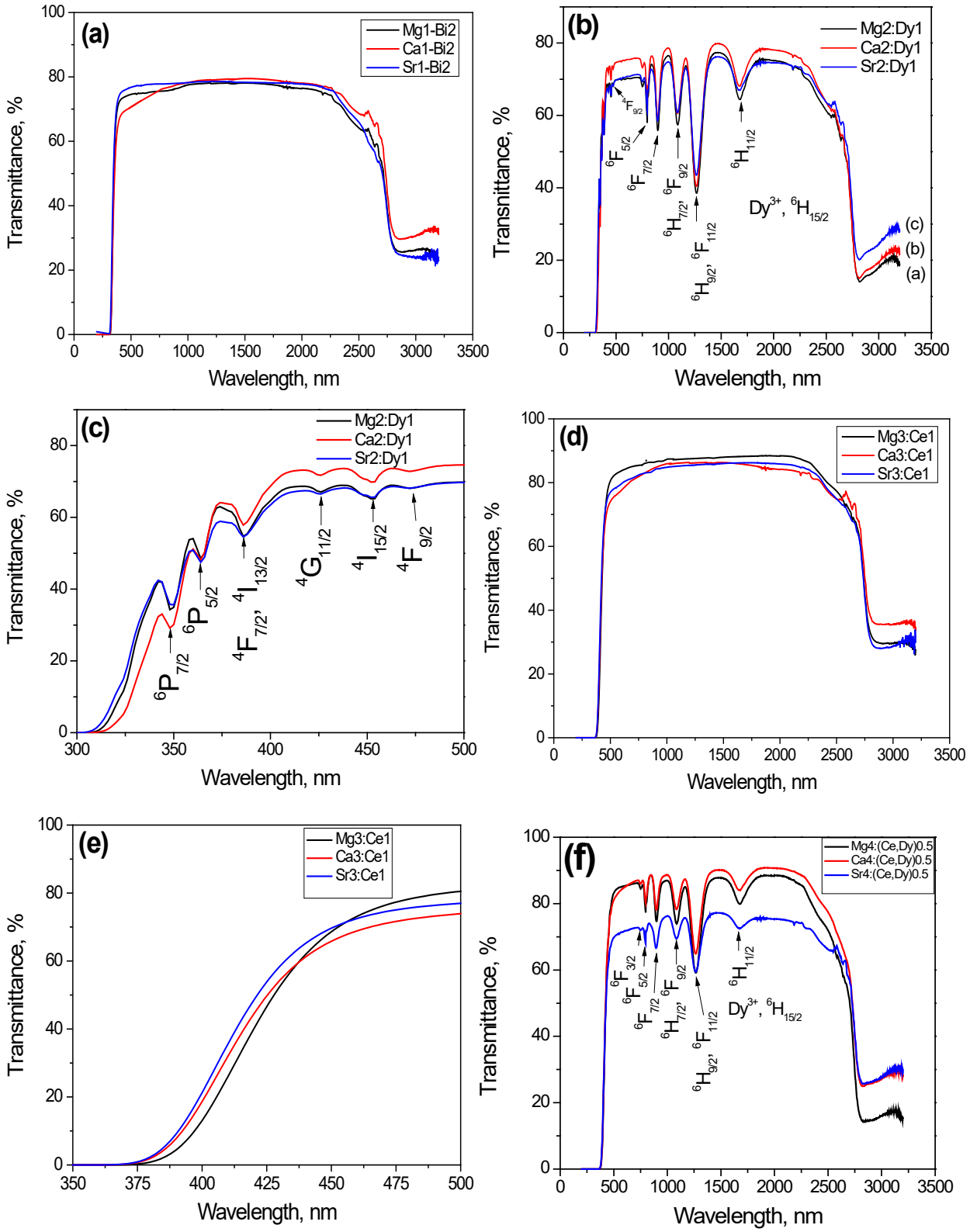

Fig. 3. Transmission spectra of studied glasses (samples thickness is presented in Table 2): (a) undoped Mg1-Bi2, Ca1-Bi2 and Sr1-Bi2; (b) and (c) Mg2:Dy1, Ca2:Dy1, Sr2:Dy1; (d) and (e) Mg3:Ce1, Ca3:Ce1 and Sr3:Ce1; (f) Mg4:(Ce, Dy)0.5, Ca4:(Ce, Dy)0.5 and Sr4:(Ce, Dy)0.5.

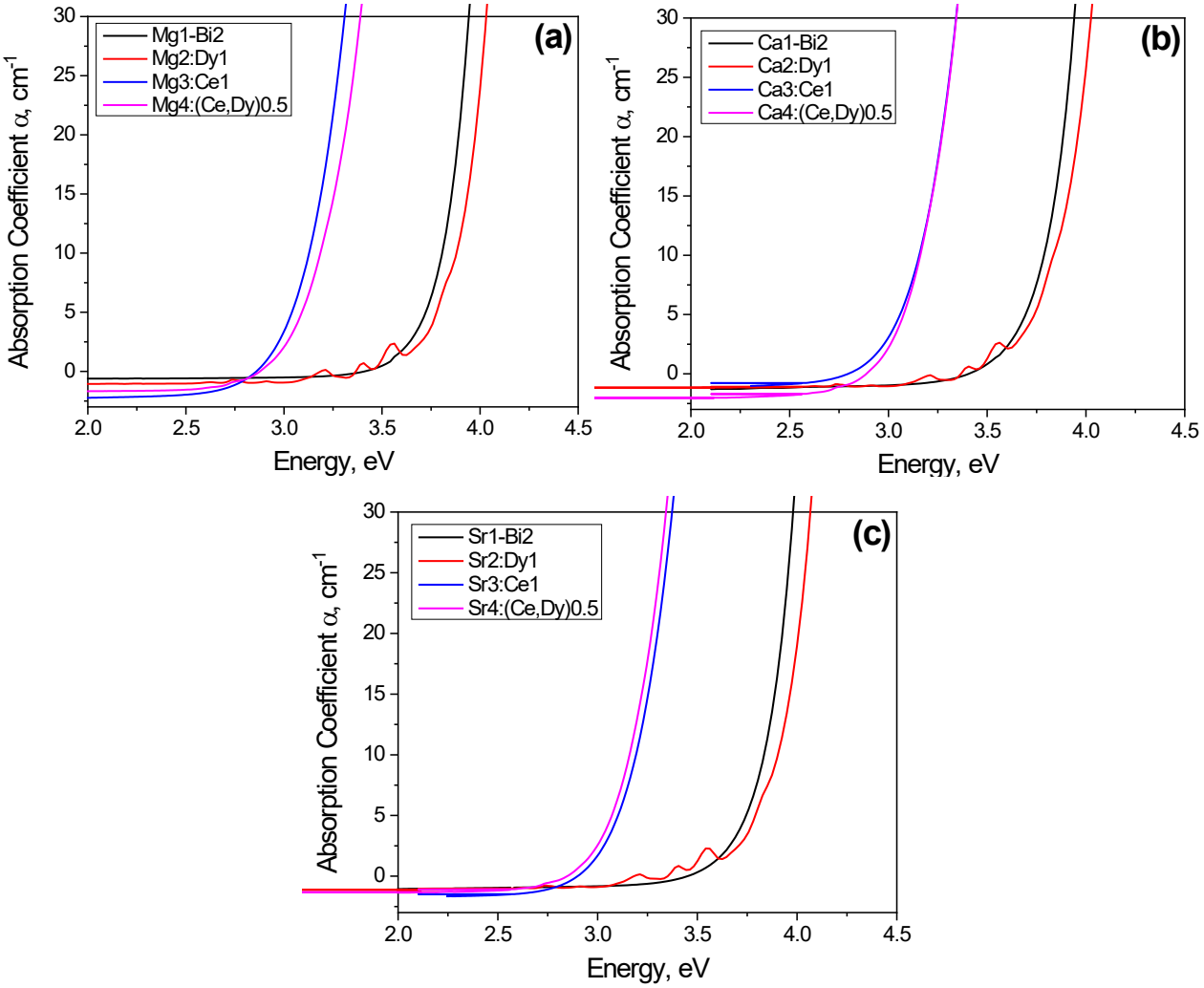

Fig. 4. Absorption coefficient spectra for the investigated series of lithium borate glasses.

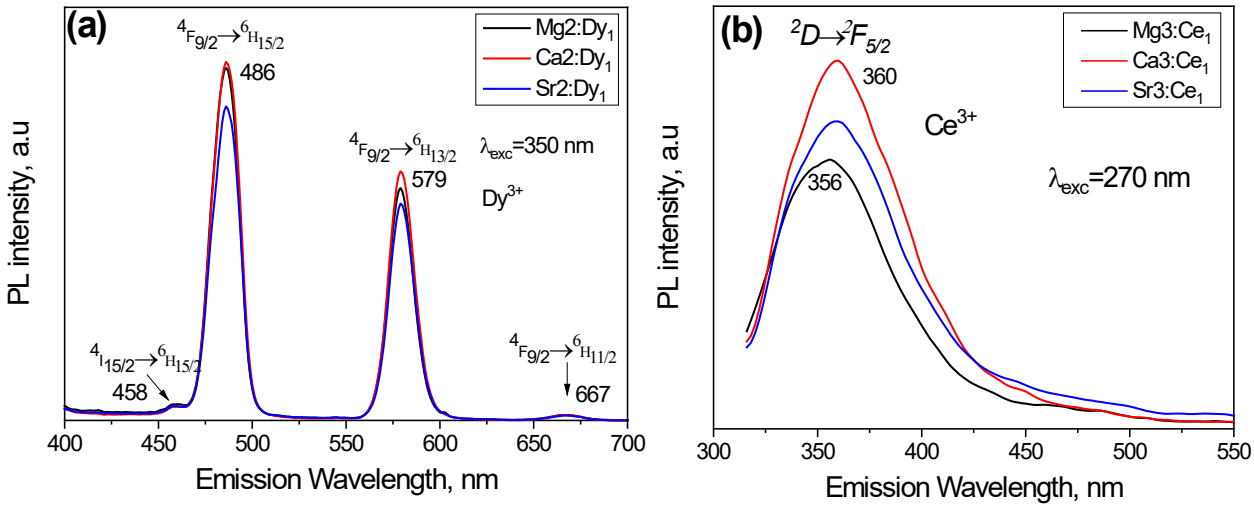

Fig. 5. Photoluminescence spectra of (a) Mg2:Dy1, Ca2:Dy1 and Sr2:Dy1 glasses under 350 nm excitation and (b) Mg3:Ce1, Ca3:Ce1 and Sr3:Ce1 glasses under 270 nm excitation.

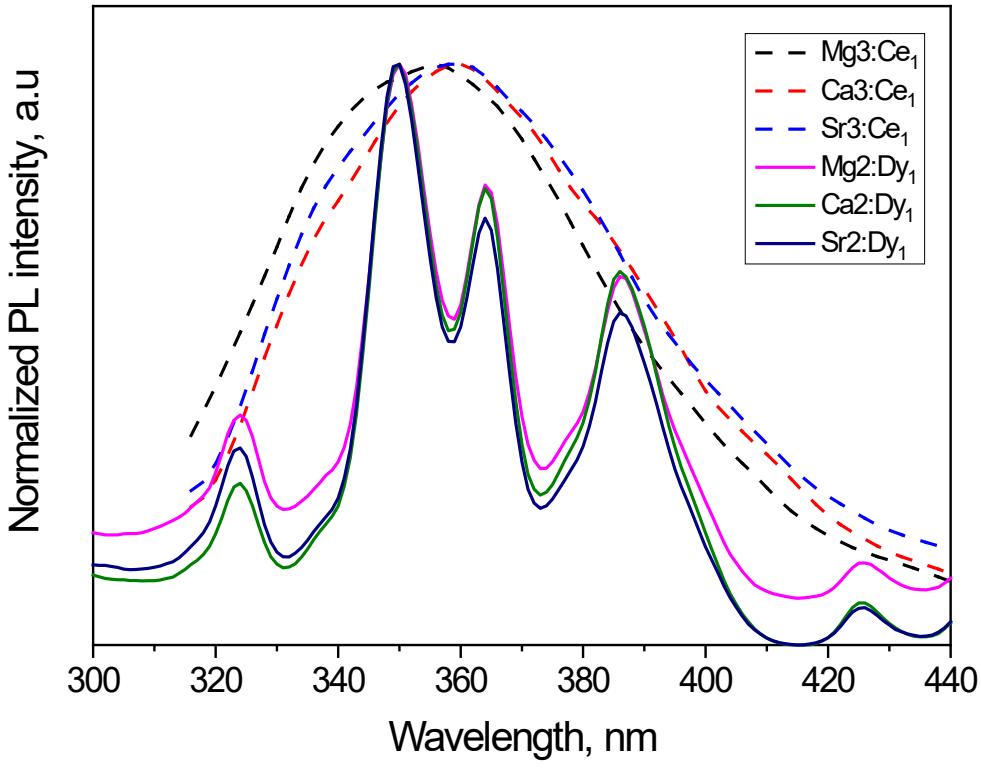

Fig. 6. Emission bands of Ce^{3+} ions (dash lines) under 270 nm excitation, and excitation bands of Dy^{3+} ions at 486 nm emission registration (straight lines) in the studied borate glasses.

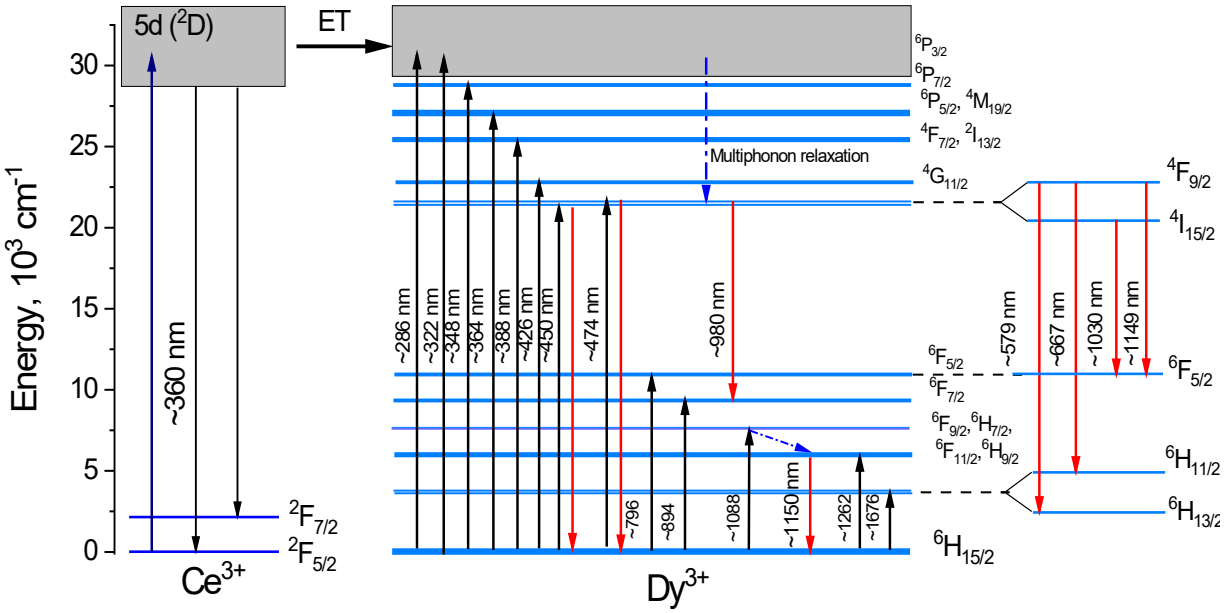

Fig. 7. Energy level diagram of Ce^{3+} and Dy^{3+} ions with their possible energy transfer.

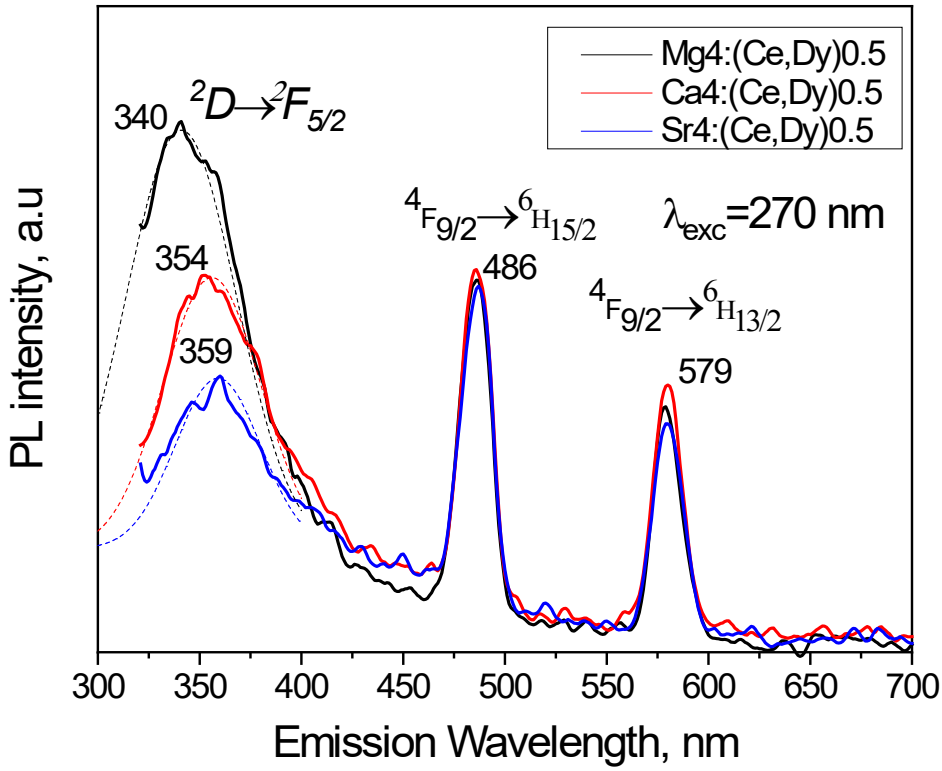

Fig. 8. Photoluminescence spectra of Ce/Dy – co-doped alkaline-earth lithium borate glasses.

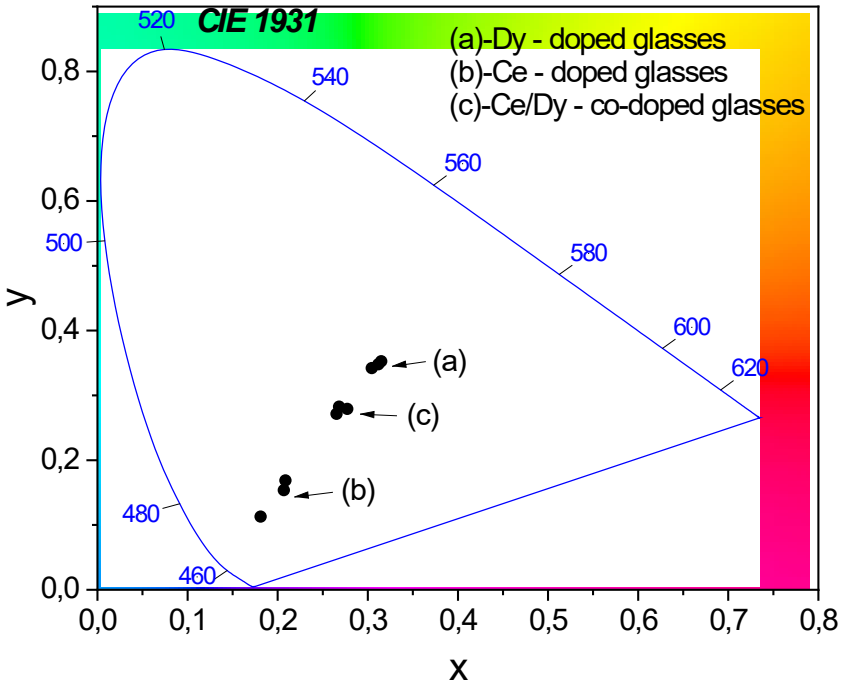

Fig. 9. CIE 1931 chromaticity diagram of Ce/Dy – co-doped alkaline-earth lithium borate glasses.

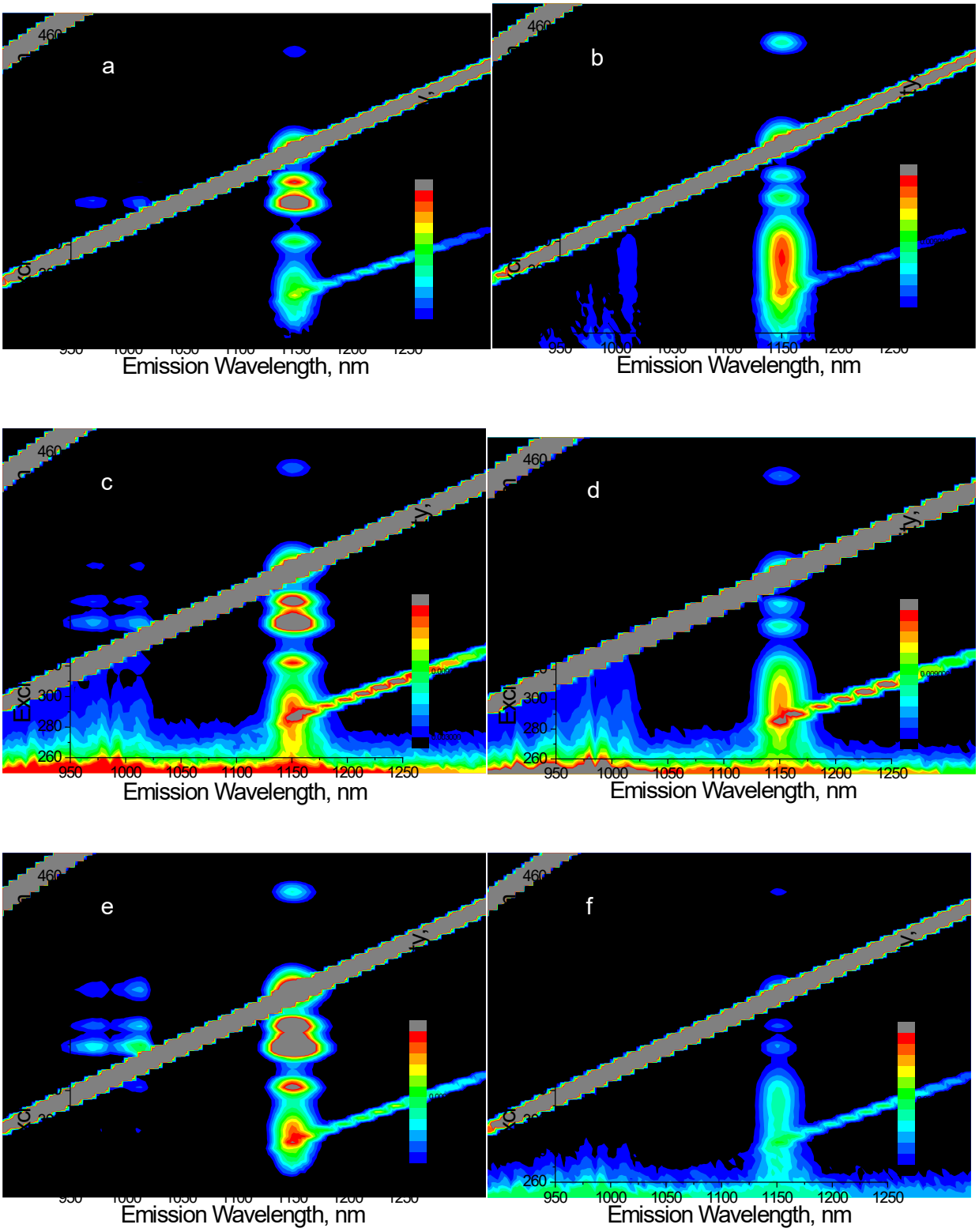

Fig. 10. Photoluminescence spectra of Ca2:Dy1 (a), Ca4:(Ce,Dy)0.5 (b), Mg2:Dy1 (c), Mg4:(Ce,Dy)0.5 (d), Sr2:Dy1 (e), Sr4:(Ce,Dy)0.5 (f) glasses in near-IR region. Lines correspond to the harmonics of Rayleigh scattering.